Open Access Journal

Journal of Power Technologies 97 (5) (2017) 359–365

journal homepage:papers.itc.pw.edu.pl

Numerical investigation of temperature distribution in the furnace of a coal fired grate boiler in part load conditions

Łukasz Więckowski, Piotr Krawczyk*, Krzysztof Badyda

Institute of Heat Engineering, Warsaw University of Technology, Nowowiejska 21/25, 00-665, Warsaw, Poland

Abstract

Gas temperature distribution along the grate length in part load conditions is expected to be non-uniform and vary significantly from the nominal. The objective of this work was to simulate the combustion process inside the furnace of a WR-25 coal fired grate boiler at two part load conditions. The results obtained were then compared to on-site temperature profile measurements taken 0.8, 2 and 3.5 meters above the grate level. Numerical analysis was performed using a commercial CFD (computational fluid dynamics) code. Boundary conditions at the grate-freeboard interface were calculated with a black-box type model. Off-design air distribution along the grate was taken into account based on real unit inspection. Model predictions demonstrated a good overall qualitative match with measured temperature profiles, but a quantitative comparison shows a need for improvements in the modeling. It was also shown that more attention needs to be paid to the modeling of soot, as it has a major impact on predicted temperatures.

Keywords: Coal firing; grate boiler; combustion; soot; computational fluid dynamics

1. Introduction

Grate firing is one of the solid fuel combustion technologies used to produce heat and power in small-sized boilers. Despite its age, it is still very popular in coal and biomass combustion. It is easy to operate, requires little maintenance and can be used to burn low quality fuel. In Poland, there are 874 grate fired hot water boilers installed in 272 district heating power plants with output power greater than 20 MW [1]. Increasingly stringent pollutant emission regulations are driving attempts to optimize even these low capacity units [2].

The moving grate is the most common type of grate used for coal combustion in district heating and in industry [3]. Fuel is fed onto the grate and is transported along the furnace. Primary air is supplied through several wind boxes from beneath the grate (typically 6–7 zones). Ignition is initiated by radiation heat flux from the ignition arch located on the front wall. According to the generally accepted mechanism, the following conversion processes take place in the fuel bed: drying, devolatilization, ignition, volatile combustion, char combustion and ash formation [4]. As the theoretical air requirement varies along the grate, reaching its maximum half way along the grate [5], primary air staging is needed (non-uniform supply air distribution along the grate zones). A global air-fuel equivalence ratio of 1.3–1.4 is typically used, but it often reaches 1.6–1.8 [3], especially for part load operation. Secondary air is often injected above the grate to improve mixing, equalize combustion gas temperatures, improve overall combustion performance and reduce pollutant emissions [3, 6]. In practice, depending on the operator, real boiler operation may differ from the theoretical (no primary air staging, only a few initial grate zones utilized instead of all, no secondary air), leading to non-uniform gas temperature distribution inside the furnace [7].

Computational fluid dynamics (CFD) have proven to be an efficient tool for modeling, design and optimization of biomass [4, 6, 8, 9, 10, 11, 12, 13, 14, 15, 16, 17] and coal [18, 6, 8] grate fired furnaces. Grate modeling takes into account gas phase turbulent combustion (already complicated) as well as complex processes occurring in the fuel layer. Since most popular commercial CFD software packages do not have any built-in models for grate combustion, separate sub-models are necessary. Both freeboard and grate models need to be coupled in order to exchange boundary conditions at the bed-freeboard interface (i.e., velocity distribution, species concentrations, temperature, radiation heat flux etc.).

In general, modeling principles are very similar for biomass and coal combustion on the grate. There are two

*Corresponding author
Email address: piotr.krawczyk@itc.pw.edu.pl (Piotr Krawczyk)

Table 1: Nominal operating parameters

Power, MW	29
Boiler efficiency, %	83
Fuel type	Coal
Fuel LHV, MJ/kg	20.5

common approaches to modeling grate processes. One is a black-box type, i.e., based on the overall mass and energy balance of the fuel layer supplied with experience and on-site measurements above the grate [6, 19]. In the black-box approach, outputs from the grate model are provided to the freeboard model as boundary conditions and only homogenous combustion processes above the grate are modeled in detail [6]. The second approach is based on detailed modeling of grate processes where governing equations are solved for both gases and solids [9, 20].

The objectives of this paper are to: (1) build a simplified CFD model for grate combustion based on the black-box approach, (2) apply the model to a 29 MW hot water coal fired grate boiler operated at part load conditions, and (3) compare the temperature distribution inside the furnace with on-site measurements.

2. Investigated boiler

2.1. Boiler characteristics

The investigated object is a 29 MW hot water coal fired grate boiler producing hot water for district heating purposes. Coal is fed onto the moving grate of 6.5 m length and 2x2.5 m width. The primary air supply system is divided into 7 uniform zones. The geometry of the furnace is shown schematically in Fig. 1. The amount of burned fuel is controled by grate speed and fuel layer height. The basic operating parameters are presented in Table 1.

Based on information from the on-site crew, secondary air is not used during normal operation. Furthermore, only three air supply zones are open in full power operation (2, 3 and 4). For part load modes below 23 MW, only two zones are open (2 and 3). Moreover, the primary air pressure distribution is never adjusted to match the theoretical air supply requirement. In this work, calculations were performed for 25 MW and 18 MW with air-fuel equivalence ratios of 1.4 and 1.5 respectively. Boiler and furnace efficiency were assumed to be the same as for nominal power. Proximate and ultimate analysis of coal is reported in Table 2.

2.2. Available measurements

Temperature measurements inside the furnace of the described boiler were carried out for a range of power ratings by [7]. The authors found out that the temperature distribution was strongly non-uniform along the grate length and that it changed with power. Continuous measurements were performed for two weeks using ceramic coated NiCr-NiAl thermocouples. Output power varied from 8 MW to 25 MW, depending on consumer heat demand. There were 14 thermocouples (see locations 1–14 in Fig. 1) introduced through openings on the side walls of the furnace. Measurements were taken 0.8, 2 and 3.5 m above the grate level and 0.7 m away from the wall. The differences between the temperatures measured on both sides did not exceed 40 K, showing no major variation across the furnace width. The second, short term verification measurement was performed for 18 MW and 25 MW using aspirated thermocouples to estimate error associated with radiation effects. The same application ports and probe depths were used, but only on one side wall as depicted in Fig. 1. The results obtained by the aspirated thermocouples were 120–170 K higher than the ceramic coated ones in the vicinity of the front wall (~1300 K). As the temperatures decreased towards the rear wall of the furnace to 900–1000 K, the difference between the two methods fell to 15–30 K. Detailed results and a discussion of them can be found in [7].

Table 2: Coal composition.

Proximate analysis, wt%				
Char	Vola	Ash	Moisture	
C	35	1	13.5	
Ultimate analysis, DAF, wt%				
C	H	O	N	S
72.5	4.8	16	2.7	1.3

Pictures showing the interior of the discussed furnace during operation are available (private communication) and examples are shown in Fig. 2. Analysis of the pictures confirms that only a few zones close to the front wall are in use. It can also be noted that it is difficult to distinguish zones where pure char combustion might occur. Over the grate flame is visible even in the rear zones, although it is not as intense as in the front part of the grate. It is also visible that the flame sticks to the front wall of the furnace. The yellow appearance of the flame indicates the presence of radiating soot particles, which can have a significant effect on radiation heat transfer [21].

In this paper, aspirated thermocouple measurements were used for comparison with numerical predictions for 18 MW and 25 MW. Due to the limited number of measurements taken with aspirated thermocouples, coated thermocouple data was used to estimate the measurement uncertainty later used in comparisons (error bars in the results section). Pictures were used to gain better insight into grate operation, guide numerical model setup and perform qualitative comparison with model predictions.

3. Modeling approach

As mentioned earlier, CFD simulation of a grate boiler requires the coupling of a fuel layer model with a freeboard combustion model. It requires matching mass, species and

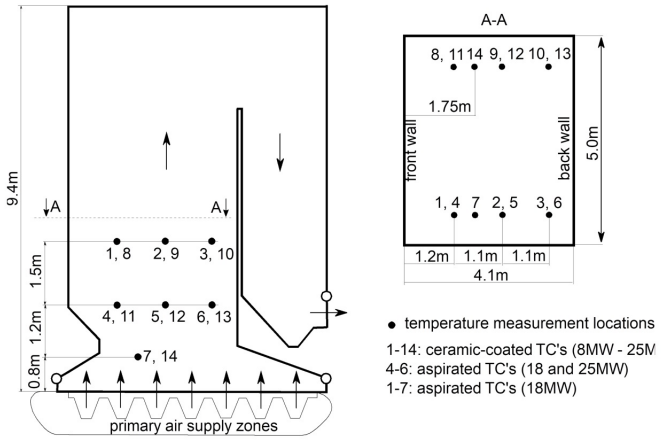

Figure 1: Schematic of the investigated boiler with marked temperature measurement locations

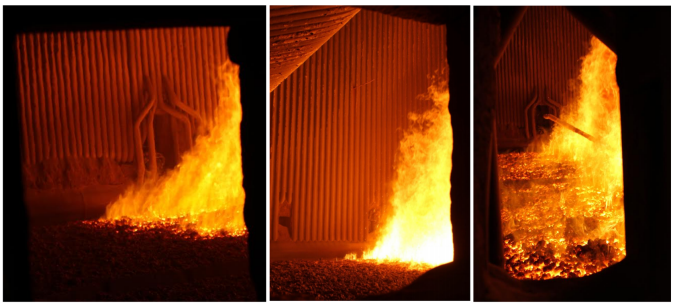

Figure 2: Pictures of investigated furnace during normal operation—view from inspection windows on the side wall. The front wall is located on the right (not visible)

energy fluxes at the interface. Here, it was achieved by solving a separate grate model and supplying its output as a set of boundary conditions for a homogenous combustion model over the bed. The combustion process above the grate was modeled by solving mass, momentum, species and energy equations for turbulent flow with heat transfer and combustion. The calculated radiation heat flux at the grate surface was then provided back to the grate model and a few iterations were performed to obtain convergence. For freeboard simulation, commercial software ANSYS Fluent was used.

The grate model was considered as a black-box. The processes occurring inside the bed were not modeled in detail—the governing equations for solid phase were not solved. The location and magnitude of drying, devolatilization and char combustion were assumed based on the mass and energy balance, which reflects generally accepted understanding as well as measurements and experience [6, 19] of solid fuel conversion on the grate. Similar approaches were used for example in [6, 13, 22].

3.1. Grate model

Due to the highly unusual nature of the investigated boiler (no air regulation, limited number of operating zones), a simple empirical submodel for grate bed conversion was developed. The output boundary conditions for the freeboard sim-

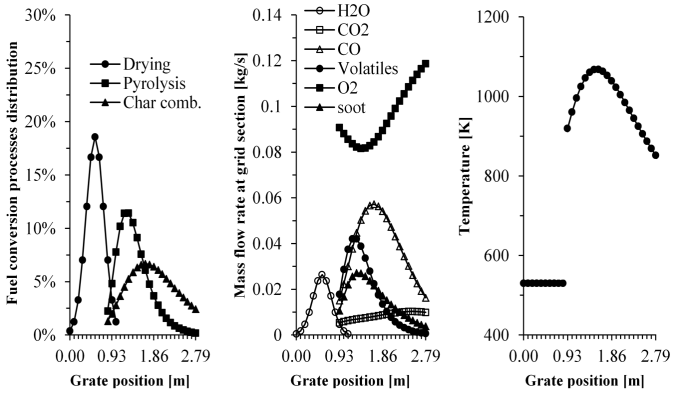

Figure 3: Example of assumed fuel conversion processes distribution, species mass flow rates through grid sections and temperature distribution on the grate for 18 MW

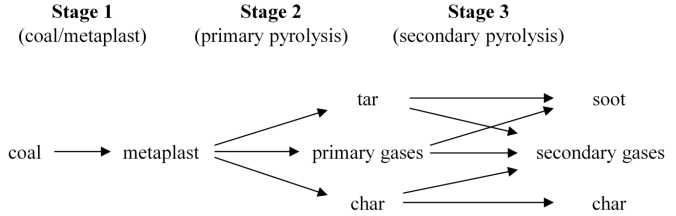

Figure 4: General scheme of coal pyrolysis—adopted from [23]

ulation consisted of velocity, temperature and species mass fraction profiles as a function of grate length. There were several inputs that needed to be provided based on real unit observation: number of primary air supply zones being open, primary air pressure distribution across the zones and grate movement velocity.

The model calculated fuel layer height based on fuel mass flow rate, grate speed, assumed bed density and rate of fuel utilization along the grate length. The packed fuel bed was assumed to be a representative set of circular tubes based on assumed porosity and specific surface area. Overall pressure losses and corresponding primary air mass flow rate distribution was then estimated taking into account known pressure loss characteristics of the grate.

In order to reflect smooth variation and overlapping of the fuel conversion processes, the grate was discretized along its length, using 10 points for each air zone. The magnitude of each process was mathematically represented using probability density function formulas. Gauss distribution was used for drying, whereas Gumbel distribution was used for devolatilization and char combustion. PDF constants were adjusted to obtain the assumed shape. Profiles were then normalized in order to sum to unity over all grid points—these values were in fact global mass fractions of a given process assigned to a local grid point. Based on these mass fractions and known fuel composition, the mass flow rate of utilized water vapor, volatiles and char was evaluated at each grid point. An example of modeled conversion processes distribution along the grate is shown in Fig. 3.

Primary pyrolysis of coal occurs in the temperature range

Table 3: Assumed volatile composition, wt%

C	C	C	C	H
6	4	1	2	1

of ~600–800 K. Tar, primary gases and char are formed. During secondary pyrolysis, in temperatures above ~800 K, tars can be cracked to gases and soot, primary gases can transform into lighter gases and soot as shown schamtically in Fig. 4 [3, 23]. According to [21], as much as 20% of a dry high volatile bituminous coal can be converted to soot, which can significantly impact gas phase radiation.

In this work, volatile matter was assumed to be a composition of secondary pyrolysis light gases: CH_4, C_3H_8, CO_2, H_2O and CO. Proportions were chosen to match the element mass balance and LHV of all the volatile content. Soot did not participate in combustion heat release, but was taken into account in radiation calculations by modifying optical properties of the combustion gases. It was assumed that the total amount of soot released with volatiles is equal to 20% of DAF coal and it was introduced at the grate-freeboard interface proportionally to the magnitude of devolatilization. It was also assumed that additional soot was released proportionally to char oxidation to CO, in the same amount as volatile soot—Fig. 2 pictures suggest that soot was released in the rear part of the grate as well. Fuel nitrogen and sulfur containing species were not included, as pollutant formation was not of interest.

Char combustion heat release was modeled using global reactions of carbon oxidation, considering both CO and CO_2 formation:

$$C + O_2 = CO_2 - 393.5 \text{ kJ/kmol} \quad (1)$$

$$C + 0.5O_2 = CO - 110.5 \text{ kJ/kmol} \quad (2)$$

It is generally understood that for char particle heterogeneous reactions, the ratio between CO and CO_2 formation grows exponentially with temperature and for temperatures above 1000 K it can be assumed that mostly CO is being formed [3]. Here, it was assumed that the ratio of global reaction rates of char oxidation to CO and CO_2 can be represented by the formula [24]:

$$\frac{CO}{CO_2} = 2500\, exp\left(-\frac{6240}{T}\right) \quad (3)$$

where: CO/CO_2—ratio of reaction rates of CO and CO_2 formation from char, T—reaction temperature [K].

The temperature of gases leaving the grate was evaluated based on energy conservation for zones where air was supplied [6]. Primary air temperature was 300 K. For the drying zone, a uniform temperature of 530 K was assumed [6]. Radiation heat flux at the grate surface was taken into account by mapping from freeboard simulation in an iterative manner until convergence was obtained. An example of the resultant temperature distribution for 18 MW is shown in Fig. 3.

3.2. Freeboard model

Velocity, temperature and species mass fractions calculated by the grate model were provided to the freeboard simulation as boundary conditions at the grate level. The temperature of the grate for radiation heat transfer was assumed to be the same as for gases leaving the grate. For grate zones where no air was supplied, as well as for the ignition arch, the adiabatic wall was assumed. The temperature of the evaporator water walls was assumed at 400 K. The emissivity of all surfaces participating in radiation was assumed at 0.9. Steady state RANS calculations were performed for gas phase combustion over the grate. For turbulence closure, a two equation realizable k-epsilon model with scalable wall functions, curvature correction and production limiter was chosen. The Discrete Ordinates model was used for radiation heat transfer with five Theta/Phi divisions and three Theta/Phi pixels. The gray gas assumption was employed. Combustion gases were modeled as an ideal gas mixture, where material properties such as density, specific heat, thermal conductivity and viscosity were calculated using ideal gas mixing law. For each individual species, density was evaluated using the ideal gas equation of state, specific heat using the polynomial function of temperature, thermal conductivity using the kinetic theory of gases and viscosity using the three-coefficient Sutherland formula. The absorption coefficient was calculated using a WSGGM cell-based model with soot effect included. To account for the fact that soot clouds have an elevated refraction index compared to non-soot combustion gases [21], a simplified approach was used—a constant value of 2 was set for the entire domain. As it was assumed that radiation heat transfer from flame was the strongest for high temperature regions that are correlated with high soot concentrations, the error associated with the constant refractive index should be low for no-soot regions. In future work, it is planned to include a soot concentration dependent function for the refractive index. The scattering coefficient was assumed to be 0.

Chemical reactions in the gas phase were modeled using species transport Eddy Dissipation Concept [25] for turbulence-chemistry interaction using standard constants. The following two-step global chemical reaction mechanism was employed with CO as intermediate specie:

$$CH_4 + 1.5O_2 = CO + 2H_2O \quad (4)$$

$$C_3H_8 + 3.5O_2 = 3CO + 4H_2O \quad (5)$$

$$CO + 0.5O_2 = CO_2 \quad (6)$$

$$CO_2 = CO + 0.5O_2 \quad (7)$$

Kinetic reaction rates were modeled using Arrhenius rate expressions with the following constants (based on [26]). Activation energy units are J/kmol and the pre-exponential factor is in SI units (ANSYS Fluent format).

$$\frac{d[CH_4]}{dt} = 5\times10^{12} exp\left(\frac{-2\times10^8}{RT}\right)[CH_4]^{0.7}[O_2]^{0.8} \quad (8)$$

$$\frac{d[C_3H_8]}{dt} = 5.6\times10^{9} exp\left(\frac{-1.26\times10^8}{RT}\right)[C_3H_8]^{0.1}[O_2]^{1.65} \quad (9)$$

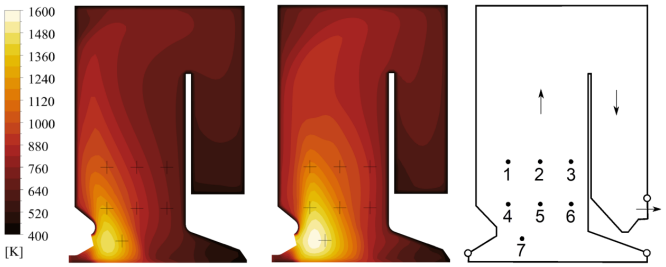

Figure 5: Temperature distribution for 18 MW (left) and 25 MW (middle) with numbered measurement locations (right)

$$\frac{d[CO]}{dt} = 2.24 \times 10^{12} exp\left(\frac{-1.67 \times 10^{8}}{RT}\right)[CO][O_2]^{0.25}[H_2O]^{0.5} \quad (10)$$

$$\frac{d[CO_2]}{dt} = 5 \times 10^{8} exp\left(\frac{-1.7 \times 10^{8}}{RT}\right)[CO_2] \quad (11)$$

4. Results and discussion

4.1. Baseline comparison with measurements

Numerical simulation of the temperature distribution in the furnace was performed for 18 MW and 25 MW. Such predictions—if validated—can be used for example to optimize the combustion process or choose optimal locations for reagent injection nozzles so as to be within the optimal temperature window for the SNCR process. A comparison of CFD results and previously mentioned temperature measurements is summarized below. An additional sensitivity study for soot modeling is also presented

Fig. 5 shows temperature contours on the cross-section where the thermocouples were placed. Temperature measurement locations are shown and numbered corresponding to Fig. 1. The model predicted that the flame tends to stick to the front wall of the furnace. It is also visible that temperatures are the highest close to the front wall and decay rapidly as the position on the grate increases, leading to a very non-uniform temperature distribution along the furnace length. This qualitative description matches real unit observations and the pictures in Fig. 2.

Fig. 6 shows a comparison of temperature profiles predicted by CFD at 2 m and 3.5 m above the grate with corresponding aspirated thermocouple measurements—thermocouples 4–6 for 2 m and 1–3 for 3.5 m. Fairly good prediction of the peak temperatures near the front wall of the furnace was achieved at 2m for both output powers—both models were inside the measurement uncertainty range. However, it is worth noting that measurement uncertainty was high compared to other locations. These measurements were taken in the region where most of the volatile combustion took place—it was therefore a region of high temperatures and high temperature gradients, as seen in Fig. 5. Temperature measurements were very sensitive to flame position, which could change due to factors such as flow field unsteadiness and space /time non-uniformity of grate processes.

As the position on the grate increased (towards the rear wall), the model started to underestimate the temperature and mismatch the measurement trend. For 18 MW, the measurements indicated that the temperature profile became almost flat close to the rear wall (thermocouples 5 and 6) at ~900 K, whereas the CFD model closely matched the measured value for location 5 and then further dropped the temperature to ~700 K in the thermocouple 6 region. For 25 MW, the measurements did not indicate any flattening of the temperature profile for thermocouples 5 and 6. The measured difference exceeded 200 K, as was well captured by the CFD model, although the predicted values were underestimated by ~50–100 K.

At 3.5 m above the grate (thermocouples 1–3), the CFD model underestimated the temperature in the front location. It also predicted monotonic temperature decay towards the back wall, whereas the measurements indicated that the temperature profile became flat for the middle and aft thermocouple. It led to a fairly good match for the middle thermocouple, but for the aft one the model prediction underestimated by ~200 K.

Thermocouple no. 7 located 0.8 m above the grate measured 1376 K, whereas the CFD model predicted 1290 K (for 18 MW). Measurement uncertainty for this location was not known.

Whereas overall predicted temperature levels were close to the measured ones, temperature distribution in the furnace missed at a few points. The authors believe the major contributing reasons to be the assumed locations and magnitudes of grate processes and overly simplified assumptions on optical properties of combustion gases. It seems that the elevated refraction index assumed in the entire domain could cause an overly strong decrease of flame temperatures—especially seen in Fig. 6 (temperature decay between thermocouple 4 and 1). This could cause the temperatures in the top part of the furnace to be underestimated, as would explain the underestimated temperatures in locations 3 and 6, because these temperatures were driven mainly by the global recirculation from the top of the furnace. There is also a question as to whether the flame position is predicted accurately—especially in the front where the flame sticks to the front wall and any displacement can introduce high errors due to the high spatial temperature gradients. The turbulence-chemistry interaction EDC model used default constants, which often require matching with experimental data. As turbulent quantities are passed to the EDC model to determine the chemical reaction rates (and thus the flame speed and position), the prediction accuracy of the turbulence field plays an important role. It is also possible that the global two-step mechanism overpredicted the flame temperatures. Then, the refractive index could be lower and still match the maximum temperatures observed in the measurements.

4.2. Soot modeling sensitivity study

Additional calculations were performed for the 18 MW case, to investigate the effect of optical properties of the

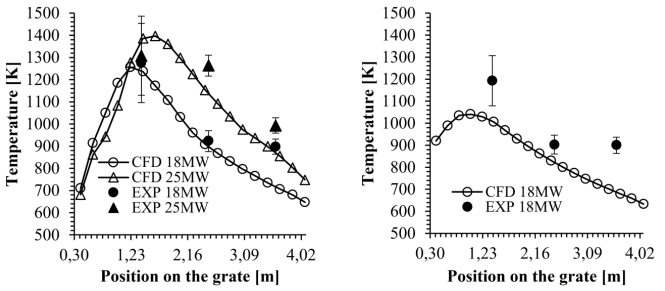

Figure 6: Comparison between CFD and measurements for thermocouples 4–6 (left) and thermocouples 1–3 (right)

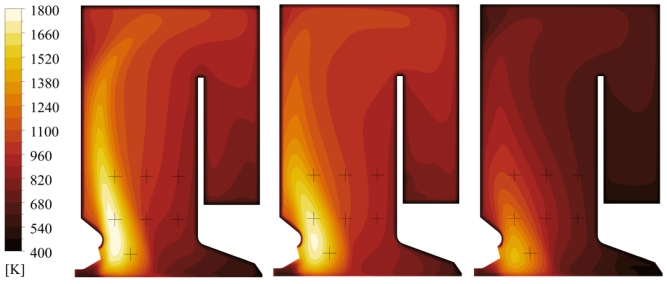

Figure 7: Temperature distribution sensitivity to various soot modeling assumptions. Soot not taken into account—case 1 (left), effect of soot included only in absorption coefficient—case 2 (middle), effect of soot included in absorption coefficient and index of refraction—baseline (right)

combustion gases on temperature predictions. The results described in section 4.1 (baseline) included soot radiation heat transfer by means of a modified absorption coefficient and refraction index. Here, the results for two more cases are presented and compared to baseline levels: case 1 without taking soot into account at all, case 2 with a modified absorption coefficient to account for soot particles, but with a refraction index equal to 1 as for non-soot gases. Fig. 7 presents the temperature contours for the three cases. As expected, taking into account the effect of soot significantly reduced maximum flame temperatures. The temperatures predicted in location 4 were as follows: 1242 K for the baseline, 1749 K for case 1 and 1677 K for case 2. The results show that modification of the refraction index had a much stronger effect on temperatures than increase of the absorption coefficient only. Case 1 and case 2 temperatures were ~475 K and ~400 K above the measurement. Even if the maximum value of the uncertainty range was considered, the difference still exceeded 200 K.

The soot modeling sensitivity study clearly showed that accurate modeling of optical properties of the combustion gases in grate combustion is crucial for correct temperature prediction within the furnace. Soot effects can have a significant impact on results and should not be neglected, as was assumed by other researchers (e.g. [8, 11, 12, 13]). The authors are naturally fully aware of the fact that assuming a constant refractive index for the soot cloud in the entire domain can lead to errors in temperature distribution prediction, but it has merit. The results presented here are preliminary. In future work, soot optical properties should be modeled in a more detailed manner, taking into account local soot concentrations for refractive index calculations.

5. Conclusions

A simplified CFD model of a coal-fired grate furnace was developed. In-grate processes were modeled using a black-box approach based on the literature, measurements and experience. The grate model was coupled with freeboard simulation, where homogenous combustion was simulated based on boundary conditions provided at the grate-freeboard interface. Comparison with temperature measurements inside the furnace was performed at various locations above the grate. An additional sensitivity study was conducted to show the importance of soot modeling assumptions, very often neglected by other authors.

While good qualitative temperature distribution in the furnace was obtained and can provide insight into grate combustion for this particular boiler, a quantitative comparison revealed that further investigation is required to build a predictive tool that is able to guide design and optimization of grate furnaces in general. Needless to say, before any pollutant formation predictions can be trusted at a predictive level, temperature distribution in the furnace has to be modeled accurately.

A CFD model tasked with design, analysis and optimization of a grate boiler (including pollutants and suppression of them) needs to consist of well validated building blocks: a grate model and gas phase turbulent combustion model. The former needs to provide accurate boundary conditions for freeboard simulation. To produce realistic results, it needs to be supplied with detailed information regarding boiler operation (primary air staging, number of working zones etc.). The latter needs to accurately predict the turbulent flow field, temperature distribution and species concentration (including pollutants). A raft of submodels need to be chosen wisely and validated both separately and in combination, including: fuel particle transport, fuel-bed heat transfer, fuel bed conversion, gas phase turbulence, gas phase combustion kinetic mechanism, turbulence-chemistry interaction, radiation heat transfer, pollutant formation/suppression. Due to the complexity and multiplicity of possible sources of error, the abovementioned building blocks need to be prioritized, developed and validated.

To build a predictive grate furnace model, detailed modeling of grate processes is required. Assumptions as to the location and magnitude of various grate processes in black-box type models may not hold for every boiler. The soot modeling sensitivity study revealed that assumed optical parameters of combustion gases above the grate have a significant impact on predicted temperatures and the uncertainty of these parameters is relatively high compared to other assumptions. These two aspects merit further investigation in the near future.

Acknowledgements

This research was supported by the POIG.01.03.01-14-035/12 project which was co-financed by the European Regional Development Fund under the Operational Programme Innovative Economy.

References

[1] P. Krawczyk, J. Lewandowski, Exploiting the potential of water boilers in poland in the light of EU industrial emissions directives (in Polish), Piece Przemysłowe & Kotły 7 (2013) 29–33.
[2] Directive 2010/75/EU of the European Parliament and of the Council of 24 November 2010 on industrial emissions (integrated pollution prevention and control), OJ EU, L 334 (17.12) (2010) 2010.
[3] E. Bulewicz, A. Dyjakon, T. Hardy, W. Kordylewski, S. Słupek, R. Miller, A. Wanik, Combustion and fuels (in Polish), Oficyna Wydawnicza Politechniki Wrocławskiej. Wrocław.
[4] C. Yin, L. A. Rosendahl, S. K. Kær, Grate-firing of biomass for heat and power production, Progress in Energy and combustion Science 34 (6) (2008) 725–754.
[5] P. Orłowski, W. Dobrzański, E. Szwarc, Steam boilers: Design and calculations (in Polish) (1979).
[6] W. Blasiak, W. Yang, W. Dong, Combustion performance improvement of grate fired furnaces using ecotube system, Journal of the Energy Institute 79 (2) (2006) 67–74.
[7] P. Krawczyk, K. Badyda, J. Szczygieł, S. Młynarz, Investigation of exhaust gas temperature distribution within a furnace of a stoker fired boiler as a function of its operating parameters, Archives of Thermodynamics 36 (3) (2015) 3–14.
[8] W. Dong, W. Blasiak, CFD modeling of ecotube system in coal and waste grate combustion, Energy conversion and management 42 (15-17) (2001) 1887–1896.
[9] Y. Yang, Y. Goh, R. Zakaria, V. Nasserzadeh, J. Swithenbank, Mathematical modelling of MSW incineration on a travelling bed, Waste management 22 (4) (2002) 369–380.
[10] H.-H. Frey, B. Peters, H. Hunsinger, J. Vehlow, Characterization of municipal solid waste combustion in a grate furnace, Waste Management 23 (8) (2003) 689–701.
[11] C. Ryu, D. Shin, S. Choi, Combined simulation of combustion and gas flow in a grate-type incinerator, Journal of the Air & Waste Management Association 52 (2) (2002) 189–197.
[12] C. Ryu, Y. Yang, V. Nasserzadeh, J. Swithenbank, Thermal reaction modeling of a large municipal solid waste incinerator, Combustion Science and Technology 176 (11) (2004) 1891–1907.
[13] C. Yin, L. Rosendahl, S. Clausen, S. L. Hvid, Characterizing and modeling of an 88 MW grate-fired boiler burning wheat straw: Experience and lessons, Energy 41 (1) (2012) 473–482.
[14] K. Goerner, T. Klasen, Modelling, simulation and validation of the solid biomass combustion in different plants, Progress in Computational Fluid Dynamics, an International Journal 6 (4-5) (2006) 225–234.
[15] T. Klason, X.-S. Bai, Combustion process in a biomass grate fired industry furnace: a CFD study, Progress in Computational Fluid Dynamics, an International Journal 6 (4-5) (2006) 278–286.
[16] S. Cordiner, A. Manni, V. Mulone, V. Rocco, Biomass furnace study via 3D numerical modeling, International Journal of Numerical Methods for Heat & Fluid Flow 26 (2) (2016) 515–533.
[17] T. Nussbaumer, M. Kiener, P. Horat, Fluid dynamic optimization of grate boilers with scaled model flow experiments, CFD modeling, and measurements in practice, Biomass and Bioenergy 76 (2015) 11–23.
[18] N. Modlinski, Computational modeling of a utility boiler tangentially-fired furnace retrofitted with swirl burners, Fuel Processing Technology 91 (11) (2010) 1601–1608.
[19] A. M. Dos Santos, R. Collin, Study of a MSW incinerator: overall operation and on-site measurements over the grate, in: National Waste Processing Conference, Vol. 15, MECHANICAL ENGINEERING PUBLICATIONS LTD, 1992, pp. 133–133.
[20] Z. Liang, X. Ma, Mathematical modeling of MSW combustion and SNCR in a full-scale municipal incinerator and effects of grate speed and oxygen-enriched atmospheres on operating conditions, Waste management 30 (12) (2010) 2520–2529.
[21] T. H. Fletcher, J. Ma, J. R. Rigby, A. L. Brown, B. W. Webb, Soot in coal combustion systems, Progress in Energy and Combustion Science 23 (3) (1997) 283–301.
[22] N. Modliński, Numerical simulation of SNCR (selective non-catalytic reduction) process in coal fired grate boiler, Energy 92 (2015) 67–76.
[23] M. A. Serio, D. G. Hamblen, J. R. Markham, P. R. Solomon, Kinetics of volatile product evolution in coal pyrolysis: experiment and theory, Energy & Fuels 1 (2) (1987) 138–152.
[24] J. Arthur, Reactions between carbon and oxygen, Transactions of the Faraday Society 47 (1951) 164–178.
[25] B. Magnussen, On the structure of turbulence and a generalized eddy dissipation concept for chemical reaction in turbulent flow, in: 19th Aerospace Sciences Meeting, 1981, p. 42.
[26] C. K. Westbrook, F. L. Dryer, Simplified reaction mechanisms for the oxidation of hydrocarbon fuels in flames, Combustion science and technology 27 (1-2) (1981) 31–43.